Available online at www.sciencedirect.com
ScienceDirect
Catalysis Today 130 (2008) 160–169
CATALYSIS TODAY
www.elsevier.com/locate/cattod

Mixed sites and promoter segregation: A DFT study of the manifestation of Le Chatelier's principle for the Co(Ni)MoS active phase in reaction conditions

E. Krebs [a], B. Silvi [b], P. Raybaud [a,*]

[a] IFP Direction Chimie et Physico-Chimie Appliquées, 1 & 4 Av. de Bois-Préau, 92852 Rueil-Malmaison cedex, France
[b] Université Pierre et Marie Curie, Laboratoire de Chimie Théorique, UMR 7616, 3 rue Galilée, 94000 Ivry Sur Seine, France

Available online 23 August 2007

Abstract

The phase diagrams and equilibrium 2D-morphologies of Co(Ni)MoS nano-crystallites with various promoter contents are determined by periodic DFT calculations coupled to a thermodynamic model. The edge energies of the crystallite depend on two key parameters: the chemical potential of sulfur ($\Delta\mu_S$), representing the sulfo-reductive conditions of the gas phase, and the number and distribution of promoter atoms at the edges.

High values of $\Delta\mu_S$, corresponding to strongly sulfiding conditions, stabilize edges with a full promoter content. At very low values of $\Delta\mu_S$, i.e. strongly reductive environment, the mixed Co(Ni)MoS active phase is destabilized with respect to MoS_2 due to the total segregation of promoter atoms to the edges. For intermediate $\Delta\mu_S$, including industrial HDS conditions, it is found that the M-edge is partially decorated by Co and Ni, and that the S-edge is partially decorated by Ni. The existence of mixed Co–Mo or Ni–Mo edge sites is thus thermodynamically possible. The Gibbs–Curie–Wulff equilibrium morphologies depend on the type of promoter. These quantitative DFT results are consistent with Le Chatelier's principle and are crucial to understand the thermodynamic balance between the active phase and the reaction conditions impacting the nature of active edge sites.

Keywords: Density functional theory (DFT); CoMoS; NiMoS; Hydrodesulfurization; Morphology; Mixed sites; Segregation effects; Le Chatelier's principle

1. Introduction

As an important insight for the evolution of the refining industry, it seems clear that the demand for middle distillate and diesel for motor fuels will remain high for the coming decade [1]. At the same time, the quality of this demand will continue to be oriented to ever cleaner products (ultra low sulfur diesel) whereas available crude oils are continuously becoming heavier. Hence, these objectives together with environmental specifications favor the implementation of new hydrotreatment processes together with conversion processes, especially catalytic hydrocracking. Hydrotreatment processes are also necessary as pre-treatment steps of vacuum gas oil to be converted by fluidized catalytic cracking or hydrocracking.

The role of research is crucial for exploring new approaches and methods for an ever better understanding and improvement of the active phases of hydrotreating catalysts. It is well known that industrial hydrodesulfurization (HDS) or hydrodenitrogenation (HDN) reactions are catalyzed by γ-alumina supported Co(Ni)MoS catalysts [2,3]. As shown by a recent review [4], the emerging technique, called ''first principles modeling'' and based on the density functional theory (DFT), has revisited existing concepts and proposed new ones useful for HDS catalysts. Among these concepts, are the atomic scale structure of the active phase, HDS reaction mechanisms on active sites, the effects of support, the ''volcano curve'' activity relationship. In particular, the role of first principles molecular modeling was crucial to understand and predict the morphology effects of Co(Ni)Mo nano-crystallites as a function of the sulfo-reductive conditions [5,6]. The concept of morphology–reactivity relationship was contained in the geometrical model of the active phase earlier proposed by Kasztelan et al. [7]. DFT calculations have thus provided a quantitative determination of

* Corresponding author. Tel.: +33 1 47 52 71 84; fax: +33 1 47 52 70 58.
E-mail address: pascal.raybaud@ifp.fr (P. Raybaud).

0920-5861/$ – see front matter © 2007 Elsevier B.V. All rights reserved.
doi:10.1016/j.cattod.2007.06.081

surface energy values and the resulting 2D-morphology of the Co(Ni)MoS nano-layer. Only scanning tunneling microscopy (STM) applied to gold supported MoS_2 and CoMoS systems [8,9] has recently brought relevant insights on the morphologies directly comparable with DFT.

The surface energy, more rigorously called ''edge energy'' in the case of the 2D shaped nano-crystallites of Co(Ni)MoS, can be calculated for the two predominant competing edges: the S-edge for the $(-1\,0\,1\,0)$ orientation and M-edge for the $(1\,0\,-1\,0)$ orientation. The earlier DFT results of surface energy as a function of the sulfo-reductive conditions (chemical potential of sulfur) were based on MoS_2 and CoMoS in 3D-periodic cells [10,11]. However, according to the crystallographic structure, more specific DFT calculations on MoS_2 and Co(Ni)MoS model clusters with relevant sizes were required to provide absolute edge energies [5,6]. Assuming a full substitution of Mo atoms by promoter at the edge [6], it was found that the Ni promoter exhibits a greater affinity for the M-edge than Co, especially in HDS conditions. In contrast, Co was more stable at the S-edge under HDS conditions. Similar DFT results have also been published by others [12].

Using the edge energies found for large Co(Ni)MoS clusters with complete edge saturation [5,6], the present work carried out on 3D-periodic slabs, explores the effects of the promoter contents and distributions at the edges on the stability and 2D-morphologies. One of the main objectives of this paper is to better determine if the sulfo-reductive conditions may lead to a partial substitution of the promoter at the edges and eventually to a full segregation of the promoter to the edge.

In the next section, we describe the methodology for calculating edge energies as a function of reaction conditions. In Section 3, the results are presented in two steps. First, the edge energies and local structures for the CoMoS and NiMoS active phases are presented as a function of the promoter content and reaction conditions. In particular, the existence of mixed sites and the full segregation of the promoter are explored. Then, the equilibrium 2D-morphologies are determined as a function of reaction conditions. In the last section, we discuss our results in light of Le Chatelier's principle.

2. Methods

All total energy calculations presented here are based on the plane wave density functional theory within the generalized gradient approximation [13,14]. Consistent with our previous works [5,6], we used the Vienna ab-initio simulation package [15,16] to solve the Kohn–Sham equations [17] within the projected augmented wave formalism [18]. The cut-off energy governing the size of the plane wave basis set is fixed at 337.0 eV. The geometry optimization is completed when the convergence criteria on forces becomes smaller than 0.05 eV/Å.

As mentioned in Section 1, the study by Schweiger et al. had explored the case of a full substitution of Mo atoms at the edge by the promoter atoms [6]. Our present study aims at extending to the case where the promoted edge is partially substituted by Co or Ni (50%). The effect on the S coverage is simultaneously investigated as a function of the reaction conditions. In order to take advantage of the previous DFT investigations [5,6], the absolute energies of the M-edge and S-edge calculated therein are used as energy reference. Periodic supercells for all promoted systems are used to calculate efficiently the energies of partially promoted edges. Thus, a large number of local configurations, S-coverages and promoter distributions, can be explored. As depicted in Fig. 1, in the $z(z')$-direction, the slab contains four molybdenum sub-surface layers capped by one row of metallic edge atoms (either Mo or Co or Ni). In the $x(x')$-direction, four nonequivalent edge sites are considered for the investigation of partial (50%) promoter edge content with two different distributions: either an alternate distribution of Mo and promoter atom (–Mo–Co–Mo–Co–), or a paired distribution (–Mo–Mo–Co–Co–). According to our previous periodic DFT calculations [10,11] and as carefully checked in this study, the corresponding cell parameters (12.29 Å, 12.80 Å, 27.01 Å) ensure a vacuum interlayer of 15.00 Å, which is known to be

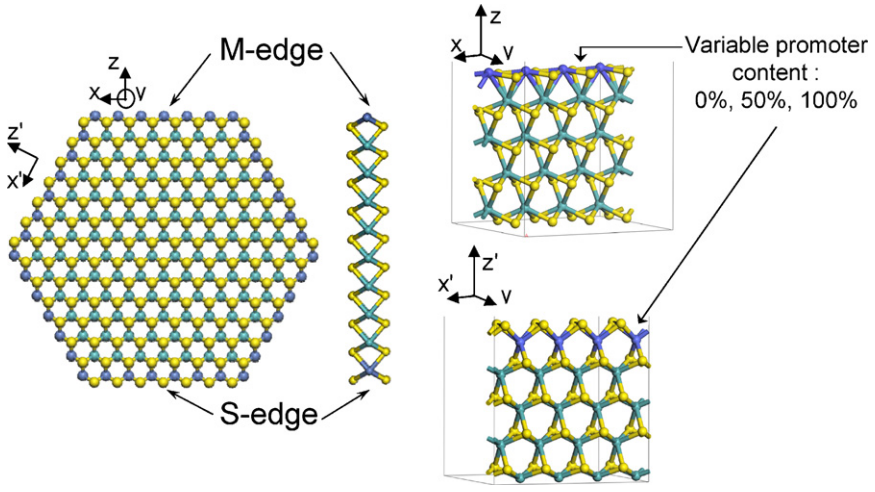

Fig. 1. Periodic slabs used to simulate the M-edge and S-edge of a promoted nano-crystallite with various promoter Me content. The stoichiometry of the slab ($Mo_xMe_yS_z$) depends on the S-coverage and Me-content (yellow balls: sulfur, green balls: molybdenum, blue balls: cobalt or nickel). (For interpretation of the references to colour in this figure legend, the reader is referred to the web version of the article.)

sufficient to avoid spurious electronic exchange between the two edges. The k-point mesh (3, 3, 1) is also optimized to ensure an accurate discrete sampling of the supercell's Brillouin zone.

Determining the stable states of the two edges in HDS reaction conditions implies calculation of the edge energies of the slab for various sulfur coverages and promoter contents. First, as shown in [10] the sulfur coverage at the edge depends on the sulfo-reductive conditions: temperature and $p(H_2S)/p(H_2)$ ratio. In particular, the higher the partial pressure of H_2S, the higher sulfur coverage of the edge [10]. In addition, the thermodynamic stability of the promoter at the edges (corresponding to the promoter edge content) also depends on the sulfiding conditions [6]. One way to solve this problem using 3D-periodic slabs is to calculate the edge energy by using the following chemical equation:

$$x\mathrm{MoS}_a\Big|_{\text{bulk}} + \frac{y}{b}\mathrm{Me}_b\mathrm{S}_c\Big|_{\text{bulk}} + \left(z - xa - y\frac{c}{b}\right)\mathrm{H_2S} \rightarrow \mathrm{Mo}_x\mathrm{Me}_y\mathrm{S}_z\Big|_{\text{edge}} + \left(z - xa - y\frac{c}{b}\right)\mathrm{H_2} \quad (1)$$

where MoS_a (MoS_2 or Mo) and Me_bS_c (Co_9S_8, Co, Ni_3S_2 or Ni) represent the reference sulfide or metallic bulk phases stable in reaction conditions. $Mo_xMe_yS_z$ is the global stoichiometry of the slab supercell used for the promoted M-edge or for the S-edge (Fig. 1). In our case, the supercell exhibits four nonequivalent edge sites, with y atoms of promoter (Me). Thus, the total number of Mo atoms (x) depends on the number of promoter atoms (y) in substitution ($x = 20 - y$). The total number of sulfur atoms is equal to z.

The variation of the Gibbs free energy for the promoted M-edge (an equivalent equation can be written for the S-edge) is written as follows:

$$\Delta G_{\text{M-edge}} = E(\mathrm{Mo}_x\mathrm{Me}_y\mathrm{S}_z)_{\text{M-edge}} - xE(\mathrm{MoS}_a) - \frac{y}{b}E(\mathrm{Me}_b\mathrm{S}_c) - \left(z - xa - y\frac{c}{b}\right)(\Delta\mu_{\mathrm{S}} + E(\mathrm{S}_\alpha)) \quad (2)$$

where $\Delta\mu_{\mathrm{S}} = \mu_{\mathrm{H_2S}} - \mu_{\mathrm{H_2}} - \mu_{\mathrm{S}_\alpha} = f(T, p(\mathrm{H_2S})/p(\mathrm{H_2}))$.

The values taken by $\Delta\mu_{\mathrm{S}}$ as a function of T and $p(H_2S)/p(H_2)$ are given by the abacus reported in [4,19]. In all following thermodynamic diagrams using this variable as abscissa, we will indicate the $\Delta\mu_{\mathrm{S}}$ range corresponding to HDS conditions.

The slabs representing the $Mo_xMe_yS_z$ edges (Fig. 1) expose simultaneously the two edges: the promoted M-edge (with various S-coverage), at the top in Fig. 1, and the non promoted S-edge (with 100% S), at the bottom in Fig. 1. Symmetrically, the second type of slab contains the promoted S-edge (with various S-coverage) at the top and the non promoted M-edge at the bottom with 0% S. Hence, the edge energy of the given edge at the top (promoted M-edge, for instance) can be deduced only if the absolute edge energy (at $\Delta\mu_{\mathrm{S}}$) for the edge energy at the bottom (non promoted S-edge with 100% S) as calculated in [5] is taken into account. In the case of the M-edge, this leads to the following expression:

$$\sigma_{\text{M-edge}}(x, z, \Delta\mu_{\mathrm{S}}) = \frac{1}{4}\Delta G_{\text{M-edge}}(x, z, \Delta\mu_{\mathrm{S}}) - \sigma_{\text{S-edge}}(y = 0, z = 100\%\,\mathrm{S}, \Delta\mu_{\mathrm{S}}) \quad (3)$$

$\sigma_{\text{S-edge}}$ ($y = 0$, $z = 100\%$ S, $\Delta\mu_{\mathrm{S}}$) represents the edge energy value of the non promoted S-edge ($x = 0$) exposed at the bottom of the slab with z value corresponding to 100% S coverage. The value was calculated in Ref. [5].

An equivalent expression is used for the S-edge:

$$\sigma_{\text{S-edge}}(x, z, \Delta\mu_{\mathrm{S}}) = \frac{1}{4}\Delta G_{\text{S-edge}}(x, z, \Delta\mu_{\mathrm{S}}) - \sigma_{\text{M-edge}}(y = 0, z = 0\%\,\mathrm{S}, \Delta\mu_{\mathrm{S}}) \quad (4)$$

$\sigma_{\text{M-edge}}$ ($y = 0$, $z = 0\%$ S, $\Delta\mu_{\mathrm{S}}$) represents the edge energy value of the non promoted S-edge ($x = 0$) exposed at the bottom of the slab with z value corresponding to 0% S coverage. The value was calculated in [5].

From Eqs. (2) and (3) it appears clearly that the edge energy depends not only on T and $p(H_2S)/p(H_2)$, but also on the promoter edge content (y) and sulfur edge coverage (z). This equation will be used to plot all edge energy diagrams in Section 3.

Using the edge energies (3) and (4), the Gibbs–Curie–Wulff laws [20,21] determine the morphology for the 2D nanocrystallites of the Co(Ni)MoS active phases (Fig. 2):

$$\frac{\sigma_{\text{M-edge}}}{\sigma_{\text{S-edge}}} = \frac{h_{\text{M-edge}}}{h_{\text{S-edge}}} = \alpha \quad (5)$$

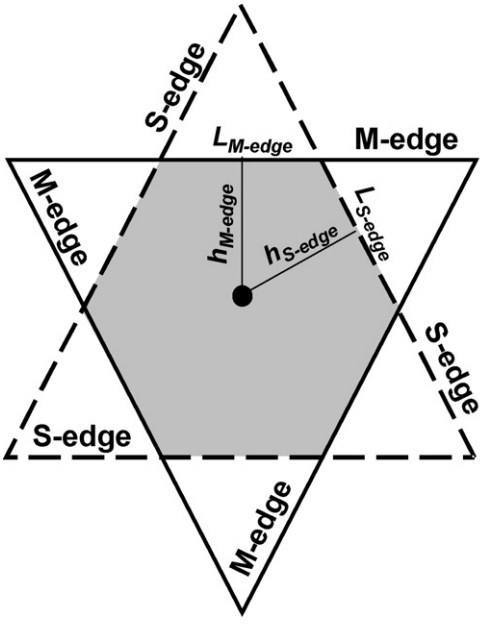

Fig. 2. Schematic representation of the 2D-construction of Gibbs–Curie–Wulff morphology of the Co(Ni)MoS nano-crystallite.

The relative distribution of the M-edge versus S-edge is deduced from the following relationship:

$$\frac{L_{\text{M-edge}}}{L_{\text{S-edge}}} = \frac{2-\alpha}{2\alpha-1} \text{ for } \tfrac{1}{2} < \alpha < 2 \quad (6)$$

Under the same conditions ($\frac{1}{2} < \alpha < 2$), the proportion of M-edge sites is:

$$X_{\text{M-edge}} = \frac{2-\alpha}{\alpha+1} \quad (7)$$

For $\alpha \geq 2$, $X_{\text{M-edge}} = 0$, the morphology is a triangle terminated by S-edges.

For $\alpha \leq \frac{1}{2}$, $X_{\text{M-edge}} = 1$, the morphology is a triangle terminated by M-edges.

For $\alpha = 1$, $X_{\text{M-edge}} = 0.5$, the morphology is a perfect hexagon terminated by an equal proportion of M-edges and S-edges.

Eqs. (5) and (7) will be used for the representation of the morphology diagrams as a function of the chemical potential of sulfur and the promoter content in Section 3.3.

3. Results

3.1. Case of the CoMoS systems

3.1.1. Edge energies

The edge energy diagrams are plotted in Fig. 3 where the values are given for the M-edge and S-edge energy as a function of the reaction conditions ($\Delta\mu_S$) for the two promoter (Co or Ni) edge contents (50% and 100%). Numerous configurations for the S-adsorption and promoter distribution at the edges have been investigated; only the most relevant configurations are reported in Fig. 4. For sake of clarity, only the edge energies corresponding to the most stable S-coverages are represented.

The affinity of the Co promoter for the S-edge and for the M-edge can be compared by considering the energy diagram in Fig. 3a. Different trends are revealed depending on the sulfo-reductive conditions. At high chemical potential of sulfur ($\Delta\mu_S > -0.6$ eV), Co reveals a similar affinity for the two edges. The values of the two edge energies for 100% Co are almost identical, which shows that a highly sulfiding regime (high $p(H_2S)/p(H_2)$) tends to equal stability of the promoter on both edges. In contrast, decrease of the partial pressure of H_2S or increase of temperature corresponding to $\Delta\mu_S < -0.6$ eV enhances the affinity of Co for the S-edge with respect to the M-edge. In particular, for typical HDS conditions ($-1 < \Delta\mu_S < -0.8$ eV), the energy of the S-edge with 100% Co is about 0.20 eV per edge metal atom lower than the M-edge. Such reaction conditions are thermodynamically favorable for Co to be located at the S-edge, in coherence with earlier results [6,22]. In addition, a new feature is revealed: a partial promoter decoration of the M-edge (corresponding to 50% Co) reduces significantly the edge energy of the M-edge, to a value close to the S-edge value. For the S-edge, the 50% Co content at the S-edge becomes energetically more favorable only for $\Delta\mu_S < -1.0$ eV. This result will have significant consequences for the morphology and the nature of active sites at the edges of the CoMoS phase.

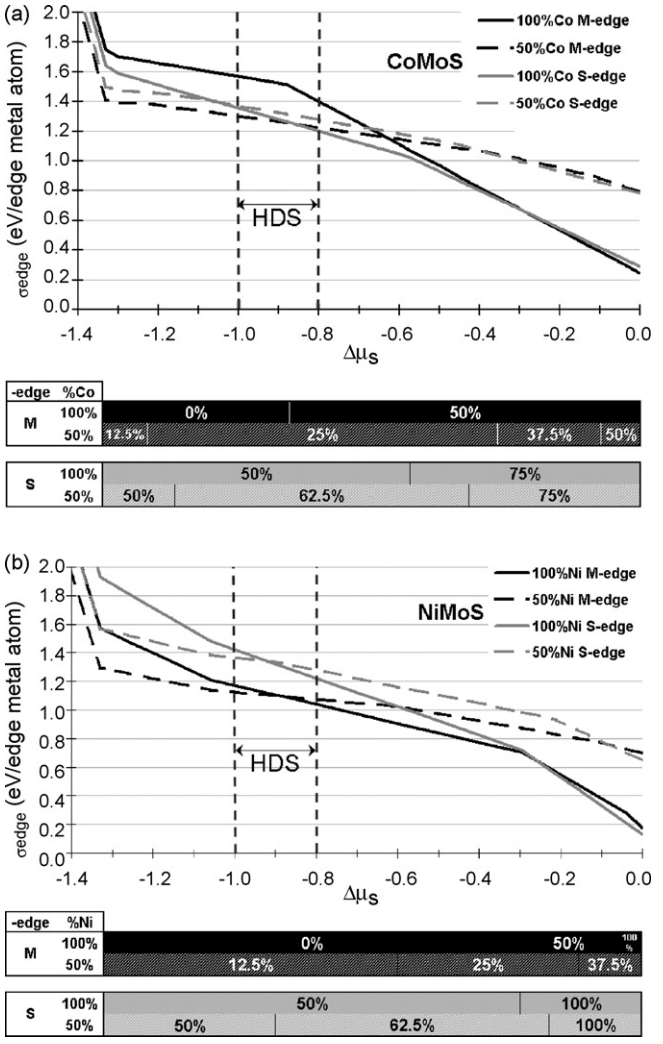

Fig. 3. Edge energy diagram as a function of $\Delta\mu_S$: (a) Co-promoted M-edge and S-edge; (b) Ni-promoted M-edge and S-edge for the two promoter edge contents (50% and 100%). The most stable S coverages for each promoter content and each edge are reported on the bar charts at the bottom of both diagrams.

3.1.2. Edge structures

The local M-edge structure with 100% Co covered by 0% S (Fig. 4a) is not thermodynamically favored in comparison to the other edge structures reported in Fig. 4. In particular, at $\Delta\mu_S > -0.6$ eV (high $p(H_2S)/p(H_2)$), the M-edge exhibits 100% Co stabilized with 50% S, as shown in Fig. 4b. For $\Delta\mu_S < -0.6$ eV, the 50% Co partial occupation with the M-edge covered by 25% S is stable. It is interesting to note that the alternate configuration –Co–Mo–Co–Mo– (Fig. 4c) and the paired configuration –Co–Co–Mo–Mo– (Fig. 4d) are close in energy (0.04 eV per edge metal atom). In both cases, the M-edge structure exhibits mixed Co–Mo sites and the S-atom sits preferentially on top of the Mo atom. The configuration of Co pairs (Fig. 4d) and the configuration with 100% Co at the M-edge by Co (Fig. 4b) are also compatible with the interpretation of magnetic susceptibility measurement by Okamoto proposing

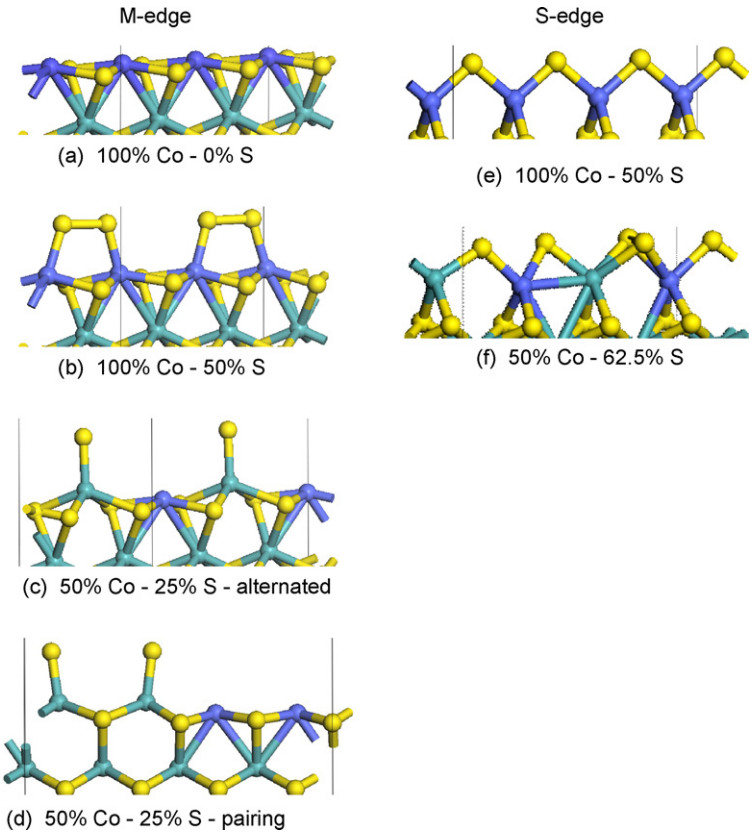

Fig. 4. Local edge structures after geometry optimization of the two CoMoS edges for the two promoter contents and the most stable sulfur coverage. (yellow balls: sulfur, green balls: molybdenum, blue balls: cobalt). (For interpretation of the references to colour in this figure legend, the reader is referred to the web version of the article.)

the existence of Co sulfide dinuclear Co species at the M-edge [23]. However, we also find that S bridging positions (not shown) are rather close in energy (only 0.08 eV higher) which means that the mobility of S-atoms on the M-edge is high. For the S-edge, the most stable structure in HDS conditions, contains 100% Co and 50% S (Fig. 4e), where Co atoms are in a tetrahedral environment confirming earlier DFT results [11,22] and STM experiments [24]. At the lower limit of HDS conditions ($\Delta\mu_S < -1$ eV), the partial decoration of Co becomes favored with a sulfur coverage of about 62.5% S (Fig. 4f). This is also a rather new feature not reported so far in the literature. In all cases (including mixed Co–Mo sites), the optimized local Co–Mo distances are comprised between 2.74 and 2.84 Å for the M-edge and are around 2.97 Å for the S-edge, which is compatible with EXAFS data [25,26].

3.2. Case of the NiMoS phase

3.2.1. Edge energies

A similar energy analysis for the NiMoS edges (Fig. 3b) reveals a different trend in the decoration of the mixed phase, especially in HDS conditions. At high chemical potential of sulfur ($\Delta\mu_S > -0.3$ eV), the energies of the two edges are almost identical. As found for the CoMoS phase, Ni decorates 100% of the edge sites with similar specific affinity for the two edges. In contrast, for $\Delta\mu_S < -0.3$ eV and especially in HDS conditions, the energy of the M-edge becomes lower than the S-edge. This trend is thus opposite to the CoMoS case. The S-edge exhibits an energy higher by about +0.2 eV per edge metal atom, which implies that Ni is thermodynamically more stable on the M-edge. This result confirms our previous calculations [6]. In addition, the new feature is that the energies of the 100% and 50% Co edge contents are identical for $\Delta\mu_S = -0.9$ eV for the two edges. As a consequence, the NiMoS phase nanocrystallites may exhibit either fully or partially decorated edges in HDS conditions. The partial decoration corresponds to the existence of mixed Ni–Mo edge sites, as described in the following paragraph.

3.2.2. Edge structures

The stable edge structures found for the NiMoS system are reported in Fig. 5. Due to the stabilization of the Ni promoted M-edge, two competing structures are relevant in HDS conditions: the fully substituted M-edge with 0% S coverage (Fig. 5a) and the partially decorated M-edge with 12.5% S coverage (Fig. 5b). In both cases, Ni is in a square planar environment as earlier proposed by DFT calculations [11]. For 50% Ni at the M-edge, the S-atom sits in a bridging position between two Mo-atoms. The strong S–Mo bond energy (significantly stronger than S–Ni) implies that the pairing configuration –Ni–Ni–Mo–Mo– is stabilized (by 0.44 eV per edge metal atom) versus the alternate configuration –Ni–Mo–Ni–Mo–, represented in Fig. 5c. This feature also distinguishes the NiMoS system from CoMoS. On the S-edge, the three most

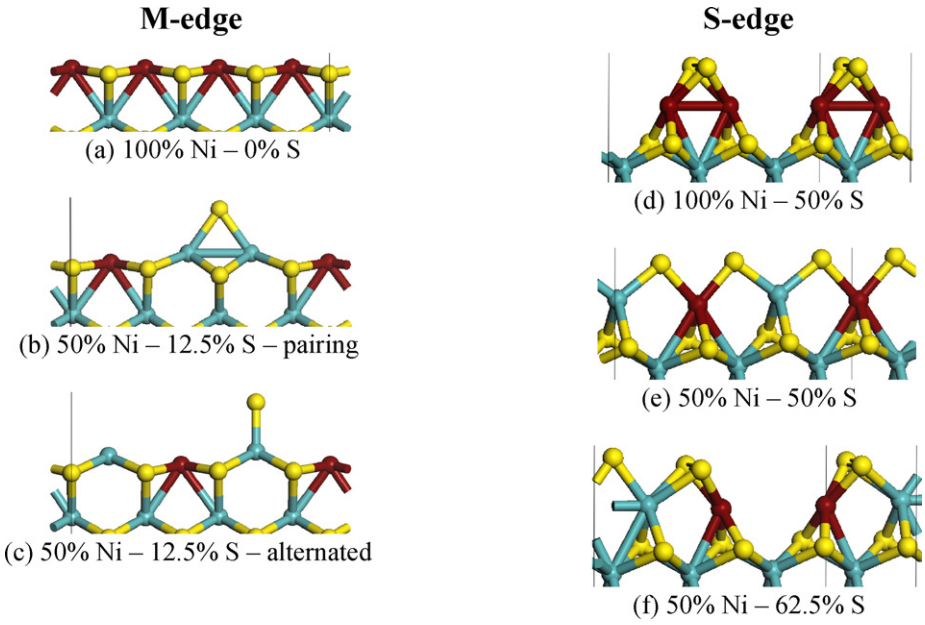

Fig. 5. Edge structures after geometry optimization of the two NiMoS edges for the two promoter contents and the most stable sulfur coverage. (yellow balls: sulfur, green balls: molybdenum, brown balls: nickel). (For interpretation of the references to colour in this figure legend, the reader is referred to the web version of the article.)

relevant structures have been reported in Fig. 5d–f. At high chemical potential of sulfur, the stable edge with 100% Ni is covered by 50% S (Fig. 5d). The local edge reconstruction leads to a square planar environment for the Ni atom, and Ni–Ni pairing. For the 50% Ni content, two competing configurations are possible. The first one (Fig. 5e) is the alternate configuration –Ni–Mo–Ni–Mo–, the second one (Fig. 5f) is a pairing configuration –Ni–Ni–Mo–Mo– where the local structure of Ni is also square planar. In all cases, the optimized local Ni–Mo distances (between 2.75 and 2.87 Å) are compatible with earlier EXAFS characterization [27,28]. The square planar environment of Ni is a key structural feature of the Ni promoter's environment which is less stable for the Co promoter. On both edges, the local structures reveal the existence of mixed Ni–Mo sites in HDS conditions.

3.3. Thermodynamic segregation at the edges

In addition to the investigation of the relative stability of the M-edge and the S-edge for a given promoter, it is also interesting to analyze the energy results for a given edge and as a function of the promoter type and content (including the non-promoted case). Fig. 6 shows this comparison, including the edge energies of the non-promoted M- and S-edges. For the M-edge (Fig. 6a), it is thus confirmed that the Co-promoted edge is less stable than the Ni-promoted edge, whatever the promoter content and reaction conditions. The most stable situation for CoMoS is found when 50% of Co atoms are in substitution of Mo atoms. In this case, the edge energy of the Co promoted M-edge is close to that of the non-promoted M-edge for $-0.2\ \text{eV} \geq \Delta\mu_S \geq -1.0\ \text{eV}$. This means that the edge energy with mixed Co–Mo sites competes with the non-promoted M-edge. For $\Delta\mu_S < -1.0\ \text{eV}$, the reductive environment or the high reaction temperature becomes a destabilizing factor for Co at the M-edge and is at the origin of the full segregation of Co to this edge. Thus, a loss of the mixed active sites located on the M-edge is suspected if the reaction conditions become too severe. In contrast, the energy of Ni promoted M-edge remains significantly lower than the value found for the non promoted system. Although the partial substitution of Ni at this edge is also competitive with the full substitution, the complete loss of Ni from the M-edge would appear at $\Delta\mu_S < -1.3\ \text{eV}$, which means that pure Ni sites or mixed Ni–Mo sites remain stable at this edge on a large range of sulfo-reductive conditions.

The analysis of the results on the S-edge leads to different features. Fig. 6b shows that the edge energies are very similar for CoMoS and NiMoS active phase. The fully promoted S-edge is the most stable in both cases over a large range of chemical potential of sulfur. The S-edge energies for 100% and 50% promoter content are identical for HDS conditions for NiMoS, and for smaller values of $\Delta\mu_S$ for CoMoS. In HDS conditions, the segregation of 50% of promoter atoms leads to the stabilization of mixed Ni–Mo sites, whereas a full Co content remains stable at the S-edge. The full segregation of the promoter from the S-edge occurs for $\Delta\mu_S < -1.05\ \text{eV}$, i.e. at the frontier of the HDS domain for both CoMoS and NiMoS. This means that the destabilization of the mixed S-edge sites phase may occur if too strongly reductive conditions are explored. Indeed, earlier Mössbauer spectroscopy characterization by Breysse et al. revealed that the mixed CoMoS phase undergoes structural modification after reaction under high hydrogen pressure and high temperature [29,30]. This observation may find its explanation in the thermodynamic segregation quantified by the larger increase of the edge energies of the CoMoS with respect to the non promoted system in such conditions.

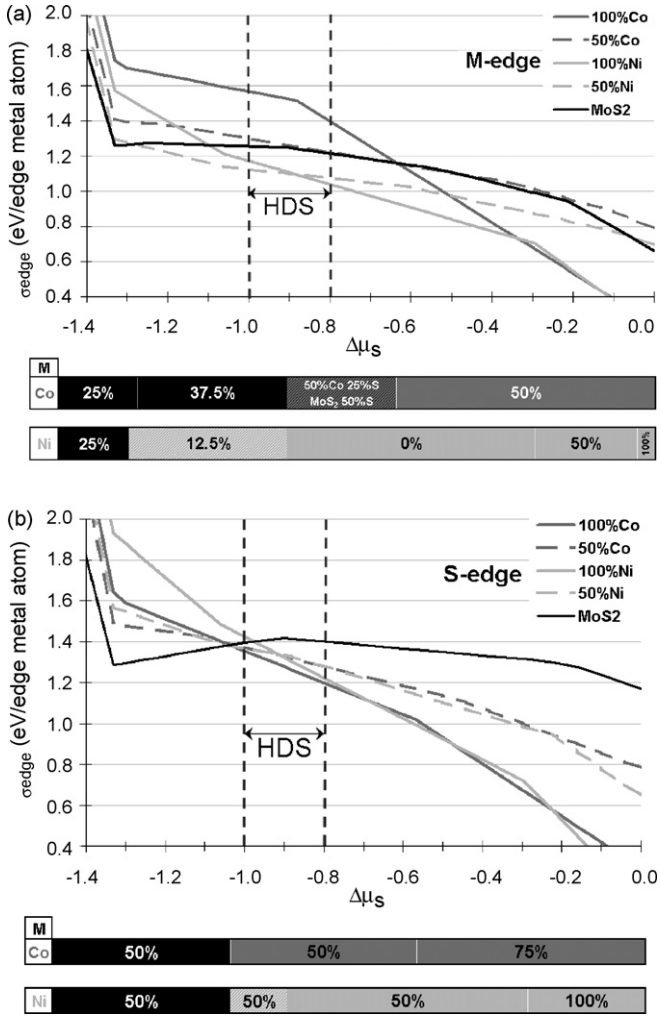

Fig. 6. Edge energy diagram as a function of $\Delta\mu_S$: (a) M-edge and (b) S-edge for the two promoter edge contents (50% and 100%) and non promoted edges. The most stable S coverages for each promoter are reported on the bar charts at the bottom of both diagrams.

3.4. Equilibrium morphologies in HDS conditions

Using the calculated edge energies and Eq. (7), the Gibbs–Curie–Wulff morphologies are determined in the diagrams of Fig. 7. These diagrams must be read as follows. The black broken line is representative of the proportion of M-edge ($X_{\text{M-edge}}$) as obtained by Eq. (7). This proportion varies with $\Delta\mu_S$, meaning that the equilibrium morphology depends on the reaction conditions or sulfidation conditions. For CoMoS, the position of this line fluctuates slightly around 0.5 indicating that the shape remains close to a hexagon (only slightly deformed). This result confirms earlier DFT trends [6] and provides new improvements including a wider range of promoter and sulfur configurations. The various domains of promoter edge content and sulfur coverage are also reported in Fig. 7. For a given reaction condition (fixed by $\Delta\mu_S$), the equilibrium shape and the composition of each edge can be deduced from the diagram. In the following Sections, we focus on HDS conditions although we are conscious that various stable morphologies and edge compositions (not drawn in Fig. 8) may be found for different reaction conditions or sulfidation conditions.

If we first consider a CoMoS nano-crystallite in HDS reaction conditions ($-1.0 \leq \Delta\mu_S \leq -0.8$ eV represented by the gray region in Fig. 7a), the proportion of M-edge is close to 0.5 (hexagonal shape). The S-edge contains 100% Co covered by 50% S (Fig. 4e), whereas the M-edge exhibits 50% Co covered by 25% S (Fig. 4c) competing with the non promoted M-edge. Assuming a typical average crystallite size of 35 Å, the two possible models for the CoMoS nano-crystallites are drawn in Fig. 8a and b. In Fig. 8a, the M-edge is partially substituted by Co, and the S-edge is fully substituted. The corresponding Co/Mo ratio is 0.29 which is very close to the optimal ratio required for catalytic activity [31,32]. In this case, it can be noticed that the number of mixed Co–Mo sites per crystallite is equal to 9 (including M-edge and corner sites). In Fig. 8b, we assume that more reductive reaction conditions have led to the complete loss of Co from the M-edge. In this case, the Co/Mo ratio of 0.20 is lower and the number of mixed sites is equal to 6 (corner sites only).

For NiMoS active phase, the variation of the morphology as a function of reaction conditions is more pronounced as indicated by the diagram of Fig. 7b. As also found in [6], the morphology at high chemical potential of sulfur exhibits the predominant S-edge (close to 0.7). In contrast, in HDS conditions (-1.0 eV $\leq \Delta\mu_S \leq -0.8$ eV), the morphology is a deformed hexagon exposing a M-edge proportion of 0.65. However, the situation is more complex, because for chemical potential value corresponding to HDS, four edge configurations compete in the gray region of Fig. 7b: these four configurations result from a combination of 100% Ni and 50% Ni either at S-edge or at M-edge. This implies that four local edge structures can be considered for the equilibrium morphology: for sake of clarity, only two of them are represented in Fig. 8c and d, even if all combinations of each type of edge are possible. Fig. 8c shows the model maximizing the number of mixed edge Ni–Mo sites (18) and minimizing the Ni/Mo ratio (0.17). The model in Fig. 8d maximizes the promoter content (Ni/Mo ratio of 0.40) and minimizes the number of mixed sites. According to the usual Ni/Mo ratio (smaller than 0.40) observed by XPS and required for best HDS activities [33,34], the working crystallites must combine edge structures allowing the presence of mixed Ni–Mo edge sites.

4. Discussion

In line with previous DFT works [5,6], it is confirmed that Co and Ni exhibit specific features in their local edge structures and morphologies under HDS conditions. The effects of the two promoters on the equilibrium morphology are not identical and are at the origin of specific active sites. In agreement, with STM observations [9] and previous DFT calculations [6,22], we confirm that Co develops a preferential affinity for the S-edge. Whereas non promoted MoS_2 crystallite with a M-edge proportion of 0.65–0.70 [5], the stable morphology of CoMoS nano-crystallites is close to a perfect hexagon due to the ‘‘surfactant effect’’ of Co atoms stabilizing the S-edge. The

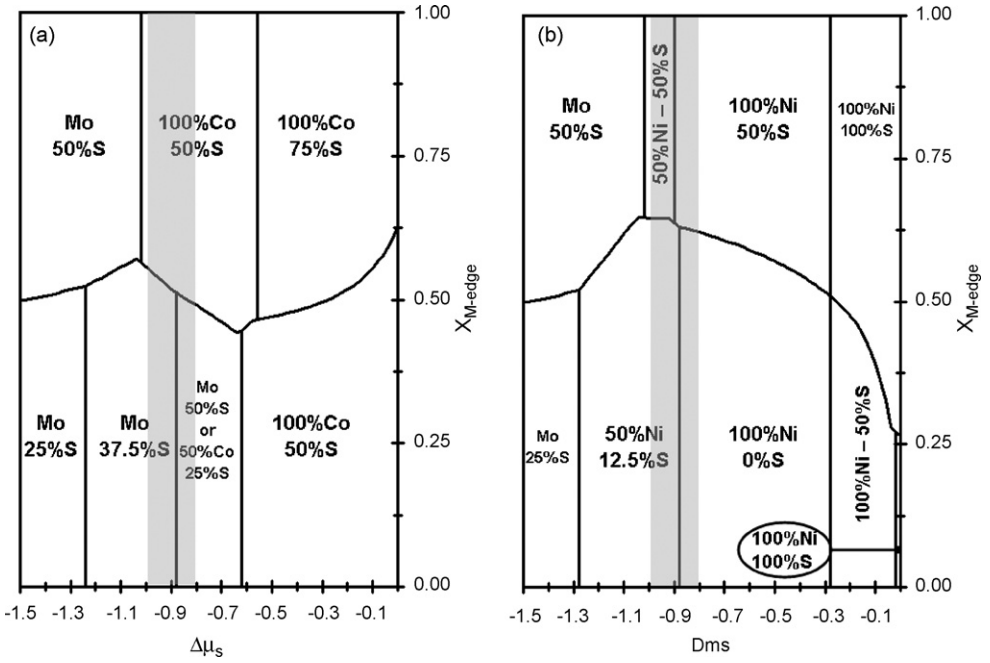

Fig. 7. Morphology diagrams for the nano-crystallites as a function of $\Delta\mu_S$: (a) CoMoS and (b) NiMoS. The proportion of M-edge (according to Eq. (7)) is indicated by the black broken line. The S-edge compositions are reported above the black line, and the M-edge compositions are below this line. The gray region visualizes the range of usual HDS conditions.

percentage of substituted Mo atoms at this edge is close to 100% according to our calculations. In addition, a new feature at the M-edge emerges. The M-edge energy calculated in the present work reveals that a partial substitution of the M-edge is possible in HDS conditions. Recent combined IR and DFT studies of CO adsorption on CoMo sulfide catalysts have suggested that low wavenumbers (below 2060 cm^{-1}) are the signature of Mo centers adjacent to promoter atoms [35], also revealing partial edge decoration. The edge energy calculations including the dependency of the promoter content are thus fully consistent with this proposal. The consequence is that the partially Co promoted M-edge exhibits mixed Co–Mo sites on the M-edge, which may be a key point in understanding HDS reactivity of the CoMoS active phase. As earlier suggested in Ref. [11], the edge S–M bond energy depends on the promoter edge content: the higher the Co content, the lower the S–M bond energy. The existence of mixed Co–Mo sites on the M-edge implies that this edge exhibits intermediate S–M bond energies required for maximizing HDS activity in line with the volcano curve relationships correlating activity and the S–M bond energy [36–38]. This interpretation applied to the role of mixed sites in toluene hydrogenation is described in detail in the paper published in this issue by Gandubert et al. [31]. Regarding the NiMoS system, the equilibrium morphology in HDS conditions is slightly more in favor of the M-edge (proportion of 0.65), which results from the higher affinity of Ni for the M-edge as found earlier in [6,12]. In addition, the refinement of the Ni edge content and distribution shows that the existence of mixed Ni–Mo sites (partial edge substitution) is energetically possible on the M-edge and S-edge, even if competition with the full edge substitution exists. This result is also consistent with the aforementioned IR and DFT studies on the NiMoS phases [35]. In the case of NiMoS, several combinations of promoted edge sites increase the number of possible reaction pathways taking place on this active phase.

It is also important to notice that there is a balance between the nature of the edge sites and the sulfo-reductive conditions. These conditions can determine both the promoter edge content and the morphology. High partial pressures of H_2S tend to diminish edge energies and to level all catalytic promoted edges which implies a maximization of the promoter edge content (close to 100% for both CoMoS and NiMoS). On the contrary, very low partial pressures of H_2S or high temperature conditions, induce complete promoter segregation to the edges and lead to complete loss of the mixed phase. Intermediate sulfo-reductive (including usual HDS) environments stabilize the presence of mixed sites, either Co-Mo or Ni-Mo sites. This behavior can also be interpreted within the generalized Le Chatelier's principle [39,40] applied to the thermodynamic balance between the catalytic active phase and its reactive environment. This balance is driven by the sulfur-metal bond energy at the edges of the active phase. According to [11], it was found that non promoted M-edge exhibit high S–Mo bond energy, whereas full Co (or Ni) promoted edges exhibit low S–Co or S–Ni bond energy. Mixed Co–Mo sites were found to exhibit intermediate S–M bond energy. The sulfur coverage at the edges depends closely on the S–M bond energy and on the H_2S partial pressure. In highly sulfiding regimes, a high sulfur edge coverage is imposed by high H_2S partial pressures. However, following Le Chatelier's principle, the catalyst tends to counteract the effect of gas phase and exposes edges with low sulfur–metal bond energy, i.e. with high promoter content. In contrast, in highly reductive conditions, low sulfur coverages are stabilized by the gas phase which implies that the catalyst preferentially exposes non promoted M-edges with high S–M bond energy in order to restrain the sulfur depletion at the edge.

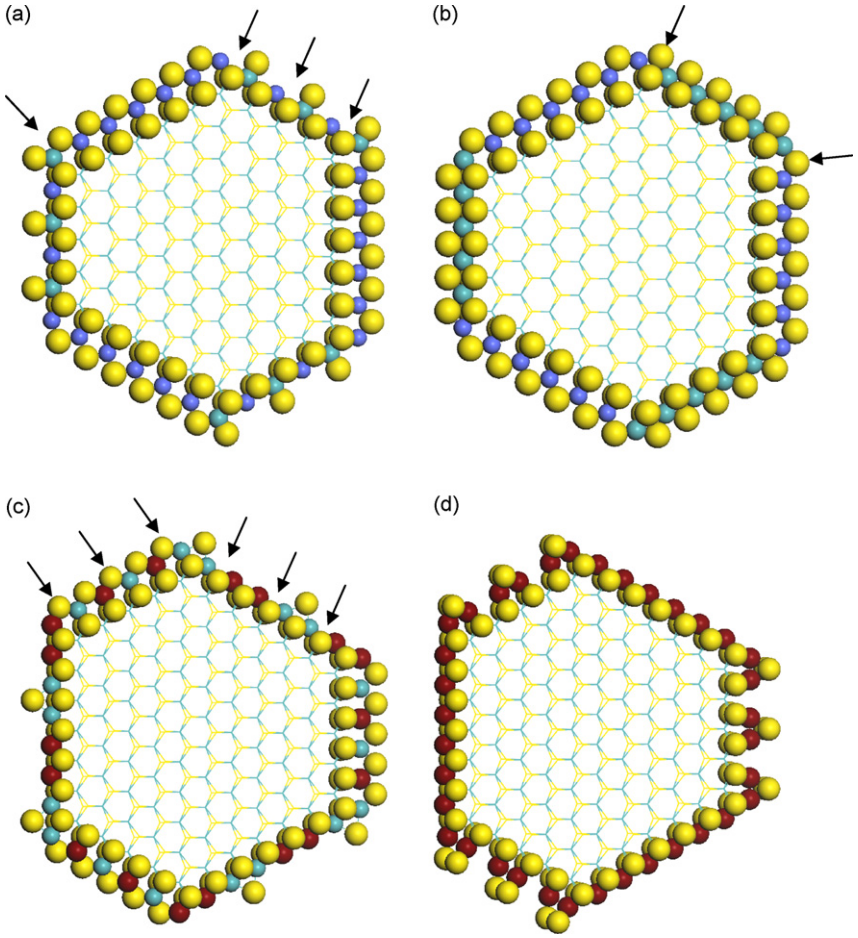

Fig. 8. Stable equilibrium morphologies and edge configurations under HDS conditions: (a) CoMoS (Co/Mo = 0.29) with 9 mixed Co–Mo sites on the M-edge and corners, (b) CoMoS (Co/Mo = 0.20) with non promoted M-edge and 6 mixed sites are at the corners, (c) NiMoS (Ni/Mo = 0.17) with 18 mixed Ni–Mo sites on both edges and corners, (d) NiMoS (Ni/Mo = 0.40) with fully substituted edges and no mixed Ni–Mo sites. Arrows indicate the localisation of some relevant mixed sites. (yellow balls: sulfur, green balls: molybdenum, blue balls: cobalt, brown balls: nickel). (For interpretation of the references to colour in this figure legend, the reader is referred to the web version of the article.)

This induces the full promoter segregation to the mixed phase. The CoMoS active phase is particularly sensitive to the negative effect of reductive conditions as also observed by Mössbauer characterization of aged CoMoS active phase [29,30]. Due to the stronger stability of Ni at the M-edge, this segregation effect mainly affects the S-edge of the mixed NiMoS phase. Finally, HDS conditions correspond to intermediate working conditions where the mixed Co–Mo or Ni–Mo sites with intermediate S–M bond energy are thermodynamically optimal for the active phases surrounded by moderate partial pressure of H_2S.

An interpretation of the role of Co–Mo and Ni–Mo mixed sites on the catalytic activity is proposed in two companion papers by Gandubert et al. and by Guichard et al. published in this issue [32,41].

5. Conclusions

The key insights obtained in the present work are the following.

- Complementary to our earlier studies [6], we have determined the equilibrium morphologies and the phase diagrams of the mixed active phase as a function of the nature of the promoter and sulfo-reductive conditions.
- Under HDS conditions, the equilibrium morphology of nanocrystallite is close to a hexagon for CoMoS, whereas it is a deformed hexagon (with a M-edge proportion of 0.65) for NiMoS.
- Ni is located preferentially in a square planar environment present at the M-edge. Local reconstruction tends to reproduce such a square planar environment on the S-edge. Co is predominantly located in tetrahedral environment at the S-edge. Ni pairing is energetically favored.
- The thermodynamic balance between the stability of promoted sites and promoter segregation effects is driven by the sulfo-reductive conditions and can be interpreted in terms of Le Chatelier's principle.
- The existence of mixed Co–Mo and Ni–Mo sites (partial decoration) under typical HDS conditions has been proven and has been interpreted as resulting from this thermodynamic balance.
- Mixed Co–Mo sites are preferentially located on the M-edge, while mixed Ni–Mo sites can be located on both edges in competition with edges fully decorated by Ni.

- Complete promoter segregation would take place under highly reductive conditions or at high temperature, which corresponds to reaction conditions generally not reached in HDT. However, this effect must be considered carefully if more severe reaction conditions are envisaged.

References

[1] E. Benazzi, C. Cameron, in: HART (Eds.), World Diesel Clean Technology, World Diesel Report: 2005, 6–11.
[2] H. Topsøe, B.S. Clausen, F.E. Massoth, in: J.R. Anderson, M. Boudart (Eds.), Hydrotreating Catalysis—Science and Technology, vol. 11, Springer-Verlag, Berlin/Heidelberg, 1996.
[3] R. Prins, in: G. Ertl, H. Knözinger, J. Weitkamp (Eds.), Handbook of Heterogeneous Catalysis, vol. 4, Wiley-VHC Verlagsgesellschaft, Weinheim, 1997, p. 1908.
[4] P. Raybaud, Appl. Catal. A: Gen. 322 (2007) 76.
[5] H. Schweiger, P. Raybaud, G. Kresse, H. Toulhoat, J. Catal. 207 (2002) 76.
[6] H. Schweiger, P. Raybaud, H. Toulhoat, J. Catal. 212 (2002) 33.
[7] S. Kasztelan, H. Toulhoat, J. Grimblot, J.P. Bonnelle, Appl. Catal. A: Gen. 13 (1984) 127.
[8] S. Helveg, J.V. Lauritsen, E. Lægsgaard, I. Stensgaard, J.K. Nørskov, B.S. Clausen, H. Topsøe, F. Besenbacher, Phys. Rev. lett. 84 (2000) 951.
[9] J.V. Lauritsen, M. Nyberg, J.K. Nørskov, B.S. Clausen, H. Topsøe, E. Lægsgaard, F. Besenbacher, J. Catal. 224 (2004) 94.
[10] P. Raybaud, J. Hafner, G. Kresse, S. Kasztelan, H. Toulhoat, J. Catal. 189 (2000) 129.
[11] P. Raybaud, J. Hafner, G. Kresse, S. Kasztelan, H. Toulhoat, J. Catal. 190 (2000) 128.
[12] M. Sun, A.E. Nelson, J. Adjaye, J. Catal. 226 (2004) 32.
[13] J.P. Perdew, Y. Wang, Phys. Rev. B 45 (1992) 13244.
[14] J.P. Perdew, J.A. Chevary, S.H. Vosko, K.A. Jackson, M.R. Pederson, D.J. Singh, C. Fiolhais, Phys. Rev. B 46 (1992) 6671.
[15] G. Kresse, J. Furthmüller, Comput. Mater. Sci. 6 (1996) 15.
[16] G. Kresse, J. Furthmüller, Phys. Rev. B 54 (1996) 11169.
[17] W. Kohn, L.J. Sham, Phys. Rev. A 140 (1965) 1133.
[18] G. Kresse, D. Joubert, Phys. Rev. B 59 (1999) 1758.
[19] C. Arrouvel, M. Breysse, H. Toulhoat, P. Raybaud, J. Catal. 232 (2005) 161.
[20] M.P. Curie, Bull. Soc. Min. Fr. 8 (1885) 145.
[21] G. Wulff, Z. Kristallogr. 34 (1901) 449.
[22] L.S. Byskov, J.K. Norskov, B.S. Clausen, H. Topsoe, Catal. Lett. 64 (2000) 95.
[23] Y. Okamoto, M. Kawano, T. Kawabata, T. Kubota, I. Hiromitsu, J. Phys. Chem. B 109 (2005) 288.
[24] J.V. Lauritsen, M.V. Bollinger, E. Lægsgaard, K.W. Jacobsen, J.K. Nørskov, B.S. Clausen, H. Topsøe, F. Besenbacher, J. Catal. 221 (2004) 510.
[25] H. Topsøe, B.S. Clausen, N.-Y. Topsøe, K.J. Pedersen, W. Niemann, A. Müller, H. Bögge, B. Lengeler, J. Chem. Soc., Faraday Trans. 183 (1987) 2157.
[26] S.M.A.M. Bouwens, J.A.R. van Veen, D.C. Koningsberger, V.H.J. de Beer, R. Prins, J. Phys. Chem. 95 (1991) 123.
[27] W. Niemann, B.S. Clausen, H. Topsoe, Catal. Lett. 4 (1990) 355.
[28] S.P.A. Louwers, R. Prins, J. Catal. 133 (1992) 94.
[29] M. Breysse, R. Frety, B. Benaïchouba, P. Bussière, Radiochem. Radioanal. Lett. 59 (1983) 265.
[30] M. Breysse, R. Frety, M. Vrinat, Appl. Catal. 12 (1984) 165.
[31] A.D. Gandubert, C. Legens, D. Guillaume, S. Rebours, E. Payen, Oil Gas Sci. Technol. Rev. IFP 62 (2007) 79.
[32] A.D. Gandubert, E. Krebs, C. Legens, D. Costa, D. Guillaume, P. Raybaud, Catal. Today 130 (2007) 149.
[33] S. Houssenbay, S. Kasztelan, H. Toulhoat, J.P. Bonnelle, J. Grimblot, J. Phys. Chem. 93 (1989) 7176.
[34] F.B. Garreau, H. Toulhoat, S. Kasztelan, R. Paulus, Polyhedron 5 (1986) 211.
[35] A. Travert, C. Dujardin, F. Maugé, E. Veilly, S. Cristol, J.-F. Paul, E. Payen, J. Phys. Chem. B 110 (2006) 1261–1270.
[36] P. Raybaud, J. Hafner, G. Kresse, H. Toulhoat, J. Phys. Condens. Matter 9 (1997) 11085.
[37] H. Toulhoat, P. Raybaud, J. Catal. 216 (2003) 63.
[38] H. Toulhoat, P. Raybaud, S. Kasztelan, G. Kresse, J. Hafner, Catal. Today 50 (1999) 629.
[39] H.L. Le Chatelier, Comptes rendus 99 (1884) 786.
[40] H.L. Le Chatelier, Annales des Mines 13 (1888) 157.
[41] B. Guichard, E. Devers, M. Roy-Auberger, P. Raybaud, Catal. Today 130 (2007) 149.